Chapter 2. Principle of Rf Multicusp Ion Source

An rf discharge at low base pressure can be categorized as being either capacitive or inductive, depending on how the rf energy is coupled to the plasma. Of particular interest here is the high plasma density of inductive discharge, also refer to as ICP (inductively coupled plasma). In these plasma generators, a time-varying magnetic field induced by the antenna coils results in an azimuthal electric field which accelerates the discharge electrons. In order to make an rf ion source operate efficiently at low pressure, the path length of the ionizing primary (energetic) electron inside the plasma chamber should be maximized to ensure copious ionization of the background gas. To achieve this, magnetic fields can be used to confine the electrons. Additionally, a magnetic multi-pole confinement scheme can be utilized to enhance the lifetime (i.e., path length) of the ionizing electron. The central region of the ion source is free of magnetic fields, a feature which enables this type of ion source to produce large volumes of uniform and quiescent plasmas. In this chapter the physics involved in the design and construction of an rf multicusp ion source will be described.

2.1 Physics of Ion Source

An ion source is defined by a plasma and an extractor. For example, the ion beam current is determined by the plasma density, the electron temperature, extracting voltage, and extractor geometry. The beam composition is determined by the composition of plasma. A plasma is defined as a neutral or quasi-neutral isotropic distribution of ions and electrons at constant potential. The most commonly used method of generating and sustaining a plasma for ion source application is by applying an electric field to a neutral gas. Any volume

of a neutral gas above absolute zero temperature contains a few free electrons. These free charge carriers are accelerated by the external electric field and collide with gas atoms or molecules, and lead to an avalanche of charged particles or a so-called discharge. Discharges are classified as dc, ac, or pulsed discharges on the basis of the sustaining electric field character. The dominant process in the discharge is ionization where energetic electrons ionize the background gas by electron-neutral ionizing collisions. A fundamental condition for the ionization is that the impact electron energy, E_e, be greater than the bounded electron energy, that is $E_e > e\phi_i$, where ϕ_i is the first ionization potential. However, the probability of ionization of a neutral atom by electron impact varies with electron energy. For efficient ionization, the electron density should be high and the electron temperature, a measure of electron kinetic energy, also should be sufficiently high. Fig. 2.1 shows the electron elastic, ionization and excitation cross-sections for Argon. It can be seen that excitation cross-section follows ionization cross-section, except that it extends to lower impact energies as the excitation threshold energy is about 11.55 eV (Lieberman and Lichtenberg, 1994). One can expect that electrons with kinetic energy in the range of 10 to 100 eV will form a plasma.

Consider a plasma at thermal equilibrium, n charged particles of kinetic energy E travel with Maxwellian distribution function (Brown, 1996)

$$f(E) = n\left(\frac{4E}{\pi}\right)^{1/2}(kT)^{3/2}e^{\frac{-E}{kT}}, \qquad (2.1)$$

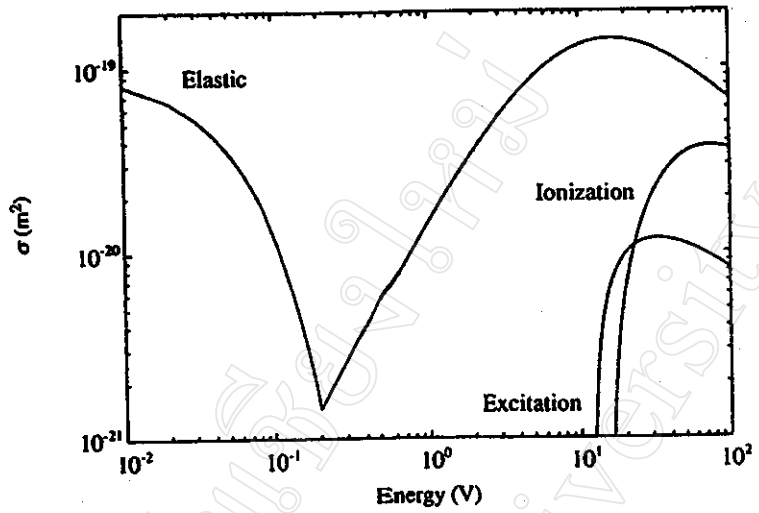

Fig. 2.1 Ionization, excitation and elastic scattering cross-sections for electrons in Argon gas (Lieberman and Lichtenberg, 1994).

where T is the plasma temperature, k is the Boltzman's constant. The mean energy of a particle is $3kT/2$. The mean free path λ, a distance where particles not collide, is related to the cross-section σ by

$$\lambda = 1/n\sigma \tag{2.2}$$

The collision frequency ν can be expressed by

$$\nu = n\sigma v, \tag{2.3}$$

where v is mean particle velocity equals to $(8kT/\pi m)^{1/2}$

From the Boltzmann relation, the density of electrons within a plasma is related to the potential, as follow:

$$n_e = n_0 exp\ (e\phi/kT) \tag{2.4}$$

Substitution of (2.4) into Poisson's equation for particles in a plasma at thermal equilibrium will yield the distance within the plasma in which electric fields are effectively excluded or shielded. This is called the Debye length, λ_D

$$\lambda_D = [\frac{\varepsilon_0 k T_e}{e^2 n_e}]^{1/2} = 743\sqrt{\frac{T_e}{n_e}}, \quad (2.5)$$

where T_e is electron temperature in eV, n_e is electron density in cm^{-3} and λ_D is in cm. For an ion source, this length is especially important in the beam formation consideration where a strong electric field is applied to the plasma from outside. For an intense ion source plasma, T_e is about 5 eV and n_e can be taken as 10^{12} cm^{-3} yielding a λ_D of $2x10^{-3}$ cm (Forrester, 1988).

2.2 Inductive Discharge

In the case of an rf inductive discharge, an electromagnetic field which is generated by a coil or an antenna permeates the discharge volume. As a result of this time-varying field, the electrons undergo cyclical accelerations and decelerations. The more massive ions do not respond to the rapidly oscillating field. Ionization takes place over the course of energetic electron collisions with the background gas during these oscillations. The equivalent circuit for a plasma in the inductive discharge is shown in Fig. 2.2. An rf current flowing in an antenna induces a plasma current with mutual inductance *M*. The plasma may be considered as a secondary winding, includes plasma resistance R_p with geometry inductance L_g and electron inductance L_e.

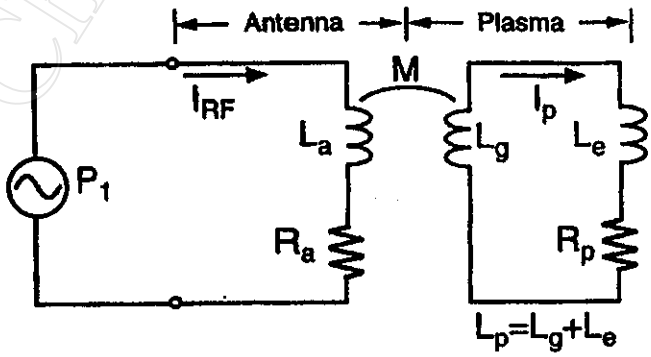

Fig. 2.2 The equivalent circuit of a plasma in the inductive discharge (Roth, 1995)

Consider the equation of motion for an electron in an alternating electric field defined by $E = E_0 \cos \omega t$ (Valyi, 1977)

$$\frac{du}{dt} + \nu u = \frac{e}{m} E_0 \cos \omega t \tag{2.6}$$

The term $mu\nu$ is the resistance of the medium due to electron collision. The electron velocity u is obtained as,

$$u = \frac{eE_0}{m(\nu^2 + \omega^2)^{1/2}} \sin(\omega t + \phi) - Ce^{-\nu t}, \tag{2.7}$$

where $\phi = \tan^{-1}(\nu/\omega)$, ω is the radian frequency. Introducing a current density per unit volume $j = n_e ue$, the power consumption per unit discharge volume is obtained

$$P = \frac{n_e e E_0^2}{m\nu} \cdot \frac{\nu^2}{\nu^2 + \omega^2} \tag{2.8}$$

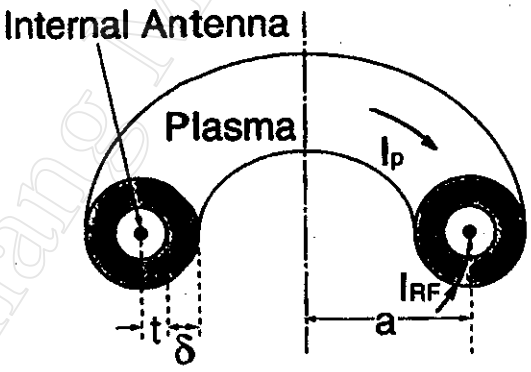

Fig. 2.3 Rf field induced by an antenna propagates through a plasma with skin depth δ_p (Roth, 1995)

In fact, an rf power is absorbed by electrons within a skin depth layer δ_p which follows when electromagnetic plane wave is damped in a medium, as shown in Fig. 2.3. For a low-pressure inductive discharge with electron density

higher than 10^{10}cm^{-3} the driving frequency $\omega << \nu$, (Roth, 1995), making it possible to rewrite (2.8) (Lieberman and Lichtenberg, 1994)

$$P_{abs} = \frac{1}{2}\frac{J_\theta^2}{e^2 n_s} m \nu \delta_p , \tag{2.9}$$

where J_θ is the amplitude of the induced rf current density, ν is the sum of collision and stochastic collision frequency. The collisionless skin depth can be calculated by the expression

$$\delta_p = \left(\frac{m}{e^2 \mu_0 n_s} \right)^{1/2}, \tag{2.10}$$

where n_s is the number of electrons in rf sheath. In the case of low pressure, maximum power transfer efficiency occurs when δ_p is about the size of the chamber. The skin depth layer of thickness 2-4 cm has been reported (Keller, 1996) at below 10 mtorr Argon pressure with an electron density in the region between 10^{10}-10^{12} cm^{-3}. It has been reported that power transfer efficiency for plasma generation using an immersed coil is much enhanced (Suzuki et al, 1998). However, as P_{abs} inversely depends on n_s (2.9), this leads to poor power absorption at high density which results in higher reflected rf power. For very low and very high density discharges, the power transfer could simply be understood as the well-known property of a transformer with an open and a shorted secondary winding, respectively. Parameters such as rf frequency, chamber size, operating pressure are interrelated and have to be taken into account when optimizing the plasma discharge efficiency.

2.3 Multicusp Field

To improve the utilization of the ionizing electrons, magnetic confinement schemes can be incorporated into the discharge process. Energetic electrons

which play major role in the ionization of atoms and molecules are more easily lost to the chamber walls than the slower ions unless steps are taken to return the fast electrons to the plasma region. It would also be of advantage to allow slow electrons having energy less than the minimum ionization energy to escape, thus reducing the possibility of electron-ion recombination. A multicusp field is widely used to confine the primary electrons. The alternating rows of permanent magnets generate a line cusp magnetic configuration in which the magnetic field strength B is maximum near the magnets and decays exponentially with distance to the center of the chamber. For alternate pole configuration, Lieberman and Lichtenberg (1994) gave the field strength at any *(x,y)* between two magnets as

$$B(x,y) = \frac{2B_0\Delta}{d} e^{-\pi y/d}, \qquad (2.11)$$

where Δ is the magnet width, d is the separation of the magnets and B_0 is the residual field strength of the magnet. The magnetic field shows an exponential decay that is independent of x with a decay length of d/π. The field is zero between the magnets and reaches the maximum value where y is about $0.28\,d$.

Most of the plasma volume confines itself in the magnetic-field-free region while a strong field exists near the chamber wall inhibiting plasma loss. This leads to an increase in plasma density and uniformity. The effects can be understood in terms of magnetic mirroring in the cusp field. The energetic electrons that are not lost by moving parallel to field lines are mirrored as they move into the higher field near the cusp. Their velocity vectors with respect to the magnetic field at the wall are randomized within the central plasma chamber. The number of reflections from a cusp depends on the size of the loss-cone angle in velocity space compared to the possible solid angle of 4π

within which the velocity vector can be found. An improvement in plasma uniformity follows because diffusion is inhibited in the region of strong magnetic field. Thus, most of the density gradient occurs at the plasma edge where the diffusion coefficient is small, leading to a relatively uniform central region. We can calculate the plasma uniformity due to the cusp field effect. If there are n cusps of width w, then the effective loss width is Nw and the fraction f_{loss} of diffusing electron-ion pairs that will be lost to the wall is (Lieberman and Lichtenberg, 1994)

$$f_{loss} = \frac{Nw}{2\pi R}, \qquad Nw < 2\pi R \tag{2.12}$$

We can use the diffusion law to relate the flux $\Gamma = nu$ to the density gradient (Fick's law) $\Gamma = -D_a \nabla n$, where n is the particle density, u is the Bohm velocity, D_a is the sum of ion and electron diffusion or so called ambipolar coefficients. We write

$$\Gamma_{wall} = f_{loss} n_s u \ , \tag{2.13}$$

and from a plasma slab of length l, we can get

$$\frac{n_s}{n_0} = \left[1 + \left(\frac{f_{loss} ul}{\pi D_a}\right)^2\right]^{-1/2} , \tag{2.14}$$

where n_0 and n_s are plasma density at $l = 0$ and at $l = l/2$ respectively, D_a is, in general, tied to the ion diffusion rate. It can be seen that the uniformity of the plasma improves as f_{loss} is reduced below unity by the presence of the cusp field. Electron density in a low-pressure plasma can be increased by a factor of 2. An average increase in plasma density of 30-80 times has been reported (Zhang, 1999). This is probably due to an increasing number of electron-atom collisions.

Fig. 2.4 shows samples of cusp field lines calculated by MAGNUS (Ferrari, 1987) which is a 3-D magnetic calculation code for Nd-Fe-B with B_r equal to 12.8 kG and for Sm-Co_5 with B_r equal to 9.5 kG magnets. The shape of the cusp field looks alike in both cases but the field strength is different. The radial variation of the field reaches a maximum of 1.8 kG at the chamber wall for Nd-Fe-B magnets. It then decreases exponentially to the source center. The calculations show a nearly field free region (<60 G) in the source center.

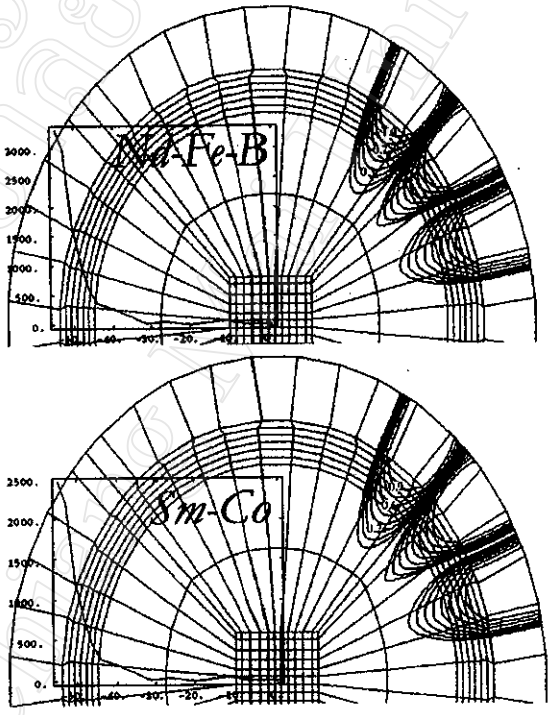

Fig. 2.4 Comparison of the calculated cusp field and field strength using MAGNUS code for Sm-Co_5 and Nd-Fe-B magnets

2.4 Beam Extraction

The formation of an ion beam depends on the extraction of charged particles from the plasma source. Since the plasma bulk is always more positive than its surroundings. Thus ions fall down the plasma potential difference with

the walls and are collected at an exit made through the plasma electrode as shown in Fig. 2.5. In a plasma source, the extraction boundary (meniscus) varies depending on the plasma density n_e and the extracting potential (Alton, 1981). Design of an extraction system starts with the desired beam current and energy *(I,V)*, plasma current density *(j)* and mass of the ion. In this case, only circular apertures and triode systems will be discussed.

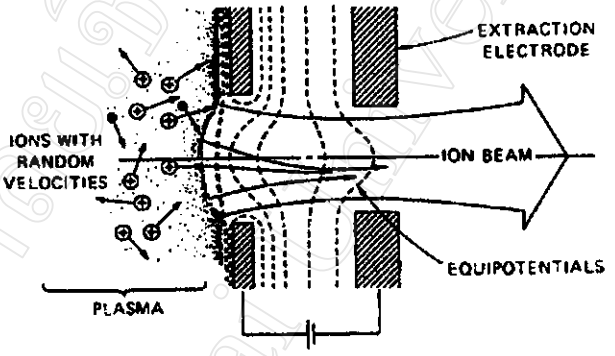

Fig. 2.5 Schematic diagram of ion extraction from a plasma source

Poisson's equation for space charge travel in a potential field is,

$$\nabla^2\Phi = -\frac{\rho}{\varepsilon_0}, \tag{2.15}$$

where Φ is an electric potential, ρ is a charge density and ε_0 is the permittivity of free space. Solving the above equation for the case of parallel plates with the following initial conditions, $\Phi = 0$ at $z = 0$ and $\Phi = V$ at $z = d$. We obtain the Child-Langmuir law as follows (see Appendix A)

$$j = \frac{4}{9}\varepsilon_0\sqrt{\frac{2q}{m}}\frac{V^{3/2}}{d^2}, \tag{2.16}$$

where V is the potential difference, d is the spacing between the planes, q is the charge state and m is atomic weight of the ion. The current density j in A/m^2 is the maximum current density that can be extracted for a giving value of d, m or

V under space charge-limited condition. In the space-charge limited regime the ion source generates more ions than can be extracted whereas in the emission-limited regime the extracting field extracts more ion than are available. In case of plasma boundary (see Fig 2.5) the extractable current density generally exhibits a $V^{3/2}$ dependence and many experimental results have derived (2.16) in the form (Alton, 1981)

$$j = \frac{C}{\sqrt{m}} \frac{V^{3/2}}{d^2} \tag{2.17}$$

where C is the source geometry dependence constant, d is the electrode spacing

In terms of perveance, P_0 which for defined beam optics, (2.16) can be written as

$$P_0 = (I/V^{3/2})$$
$$= 1.7x10^{-7}(Z/A)^{1/2}(a/d)^2 \quad AV^{-3/2}, \tag{2.18}$$

where a is the aperture radius and Z/A is charge to mass ratio. It is suggested that for a minimum beam divergence, the optimum perveance should be about 0.45 to $0.5P_0$. (Shubaly, 1987).

There are two other factors which constrain the design, one is maximum operating voltage in the gap given by

$$V_b = kd^{1/2}, \tag{2.19}$$

where d in cm, and a suitable k for Argon is $5x10^4$ (Shubaly, 1987). The second factor is the voltage breakdown which is also limited by gas pressure in the gap, known as the Paschen curve. In general ion source operation, the operating pressure is lower than 10^{-4} Torr, where the curve (Fig. 2.6) assumes high dielectric strength.

To obtain good beam optics for the system, the gap *d* should be greater than or equal to twice the aperture radius *a*. Because the angular divergence, ψ, for a circular aperture of radius a is found to be $\psi \sim a/3d$, then a reasonable choice is *d* equal to 2.25*a*. The greater value of *d* means a decrease in extractable beam intensity.

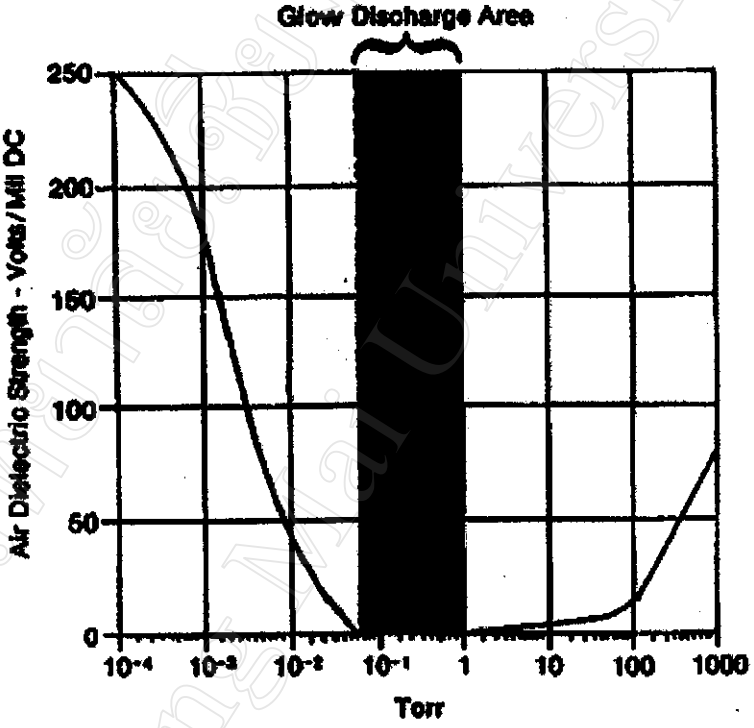

Fig. 2.6 The Paschen curve of air dielectric strength range at varied pressure (Perkins, 1997)

The addition of an intermediate electrode, between the ground and the extracting electrodes, forms an accel-decel scheme. The sufficient negative bias on this electrode prevents electrons from being accelerated away from the space charge neutralization region (plasma-ion boundary). Also it prevents electrons from back streaming when ions hit the background gas or chamber part. This electron current is normally 100 times over the ion current

2.5 A 13.56 MHz Multicusp Ion Source

An rf multicusp ion source was designed and constructed to meet the mentioned requirements. It is a modified version of the CMU 13.56 MHz multicusp ion source (Boonyawan et al, 1999) as shown schematically in Fig. 2.7. The ion source chamber is made of a stainless steel cylinder 10 cm in diameter and 9 cm long. The inner wall is surrounded by 20 columns of Nd-Fe-B magnets to form a longtitudinal line-cusp field configuration. The magnet size is 10 mm on a side by 38 mm long with residual strength B_r = 12.8 kG. They are coated with Al_2O_3 to prevent corrosion by cooling water.

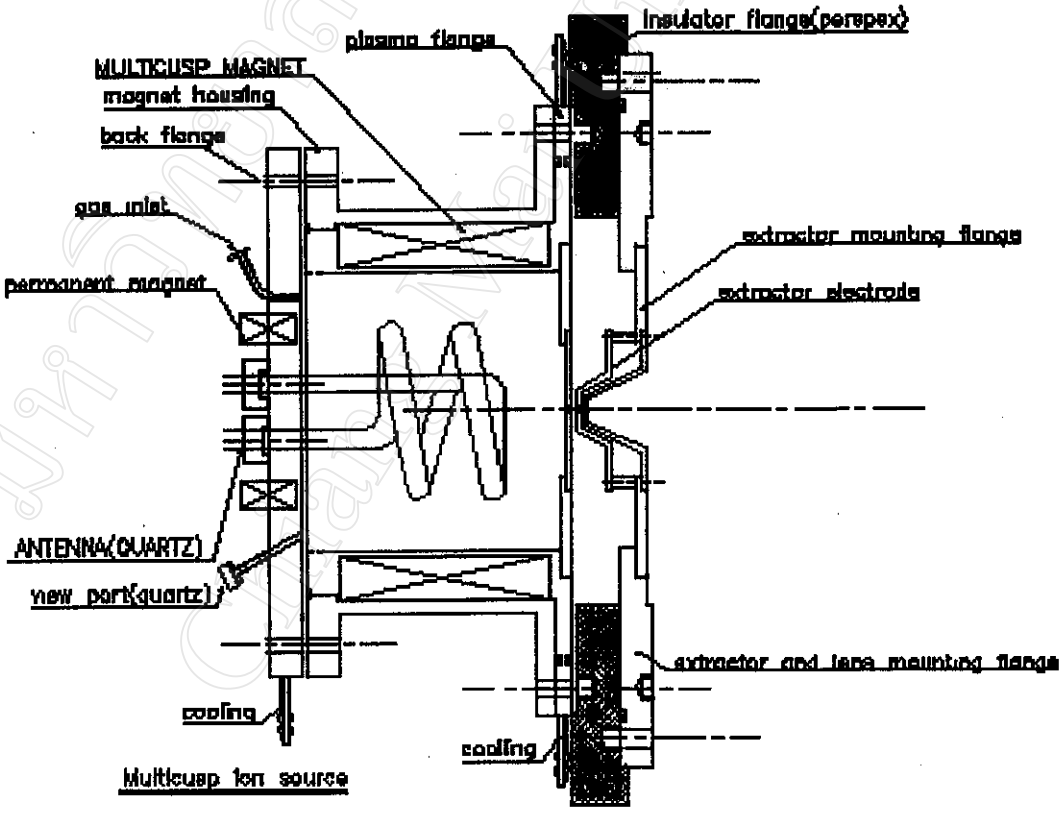

Fig. 2.7 Rf-multicusp ion source developed for high-intensity Ar beam production operates at 13.56 MHz

Fig 2.8 shows 20 rows of Nd-Fe-B magnet installed around the source chamber to produce the multicusp field. The inner wall thickness was only 2 mm to maximized field strength. Cooling water flows between pairs of magnets to protect magnets from plasma heat. The back flange is attached by 2 more magnets to complete the cusp field line. The gas inlet, the antenna feedthroughs, a pressure monitor and a view port are installed in the back flange. The plasma flange is for the plasma electrode holder; the extractor mounting flange is for extracting electrodes. Both are isolated by the insulator flange.

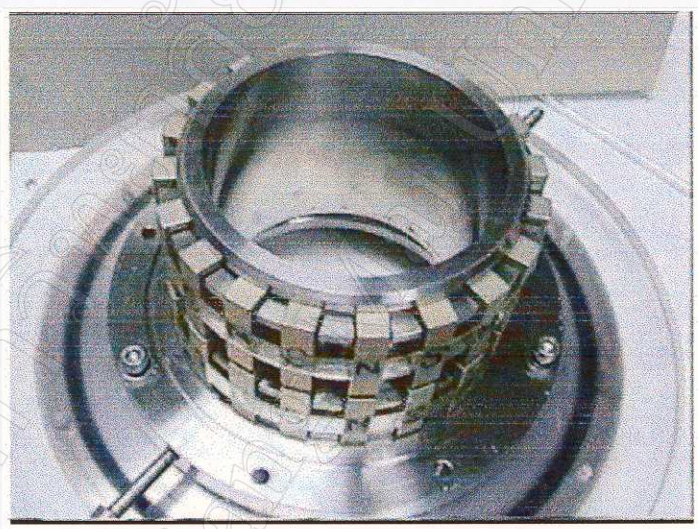

Fig. 2.8 20 rows of Nd-Fe-B permanent magnets were installed around ion source chamber to produce multicusp field

The rf power is transferred via an L-C matching box directly coupled to the plasma by an rf antenna immersed inside the source chamber. The quartz antenna, as shown in Fig. 2.9, is installed on a back flange to feed rf power to the plasma inside the source volume. The antenna coil is made of a braided copper wire threaded through a two-turn quartz tube wound in 6 cm diameter.

This antenna can handle higher rf power than a Pyrex version and can generate clean plasma compared to the bare copper antenna. Because of the low power operation (less than 500 watts) no active cooling is employed for this antenna. The dissipated power around the antenna leg outside the ion source was by forced air to protect the two vacuum o-rings in the antenna feedthrough from overheat.

Fig. 2.9 A 2 turns, 6 cm in diameter quartz antenna was installed on the back flange supplies rf power to the plasma inside the source volume

Rf power from ENI 13.56 MHz rf generator model OEM-12A[(i)] is delivered to the ion source through a matching box via a flexible, RG-213 coaxial cable of 50 ohms nominal impedance. A matching box which includes inductor and variable capacitor is placed between the rf generator and the antenna to match the loaded antenna impedance to 50 ohms output impedance of the rf generator. ----------

[(i)] ENI Power System Inc. USA

The matching circuit working at 13.56 MHz is illustrated in Fig. 2.10. A variable capacitor (10-60 pF) is used because of the plasma impedance is variable, depending on gas pressure and rf power (Piejak et al, 1992). A high frequency 30 kV isolation transformer is added to let the rf generator operate at ground potential and to function as a 10:1 step-down transformer. Thus, for this ratio, the secondary rf current is 10 times higher than the primary side, while the rf voltage is 10 times lower. This lower rf voltage on the secondary side reduce the potential for high voltage breakdown in high rf power operation. Fig. 2.11 and 2.12 show measured radial and source inner wall magnetic field strength. It can be seen that the values are almost equal to the predicted value calculated by MAGNUS.

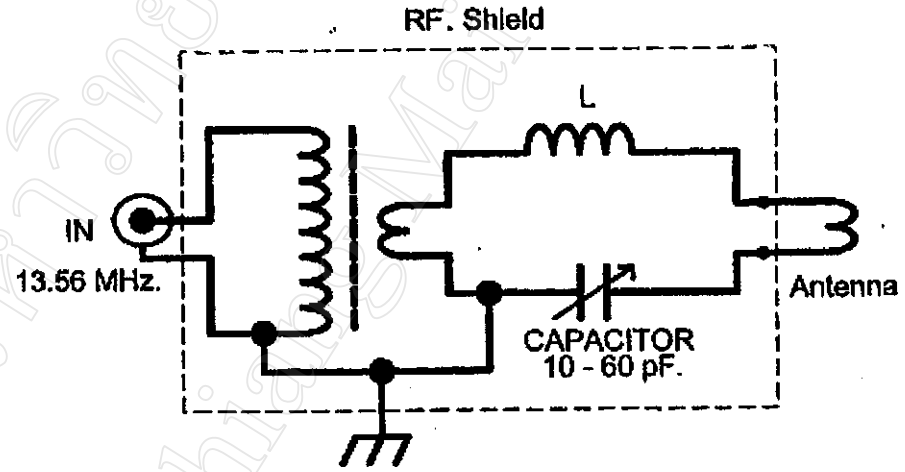

Fig. 2.10 The matching network working at 13.56 MHz includes a 10:1 transformer, a variable capacitor and an inductor in a shielded box

A typical result of Ar plasma confinement, performed at 50 watts rf power, 10 mTorr pressure is shown in Fig. 2.13. Because the Ar plasma is luminous it is possible to confirm plasma uniformity by visual inspection. It can be seen that the confinement effect to the plasma is uniform.

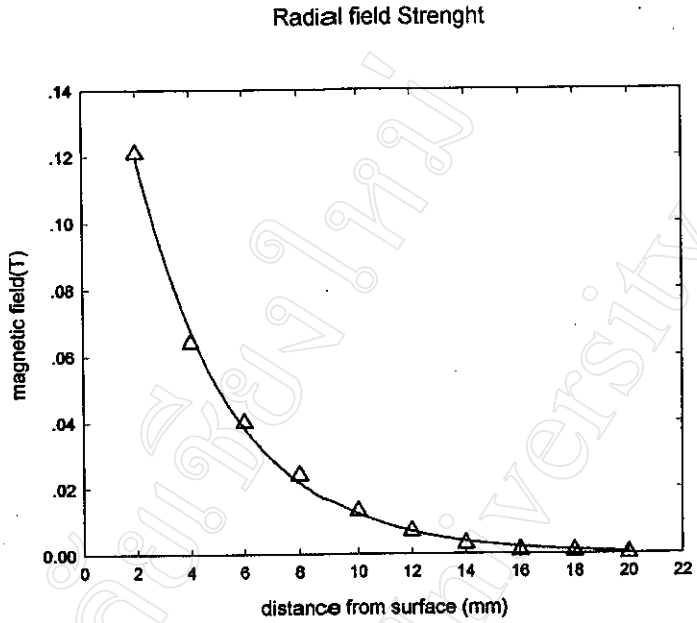

Fig. 2.11 Measured radial B field strength of 0.18 T was found maximum at the source inner wall (r = 0)

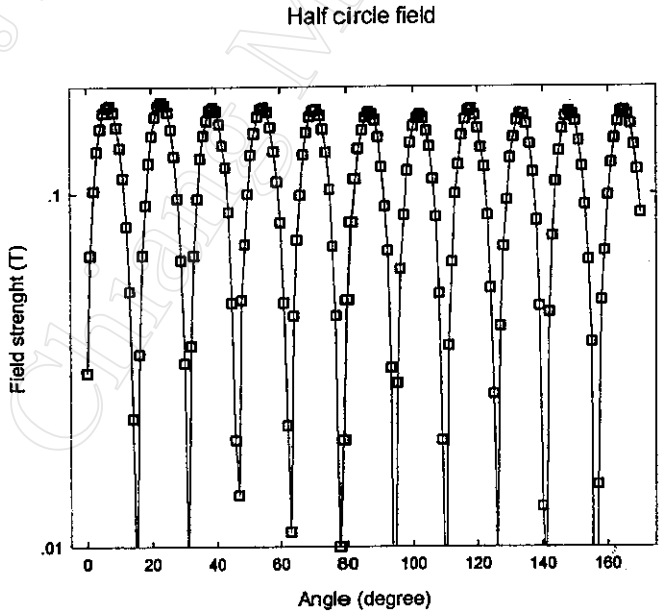

Fig. 2.12 Measured multicusp field for half circle at the source inner wall: starting between 1st magnets pair and end between 10th magnets pair

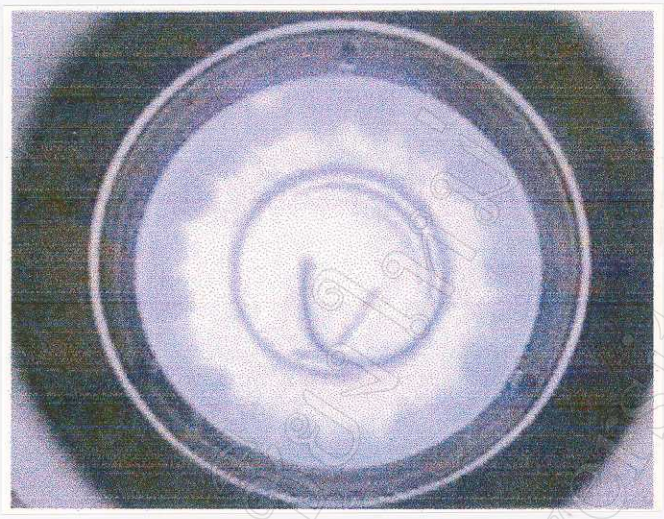

Fig. 2.13 A sample of Argon plasma confinement result seen inside the source chamber: 50 watts rf power, 10 mTorr Argon pressure